



TITLE:

Evaluation of [ $^{18}\text{F}$ ]pitavastatin as a positron emission tomography tracer for in vivo organic transporter polypeptide function

AUTHOR(S):

Yagi, Yusuke; Kimura, Hiroyuki; Okuda, Haruka;  
Ono, Masahiro; Nakamoto, Yuji; Togashi, Kaori;  
Saji, Hideo

CITATION:

Yagi, Yusuke ...[et al]. Evaluation of [ $^{18}\text{F}$ ]pitavastatin as a positron emission tomography tracer for in vivo organic transporter polypeptide function. Nuclear Medicine and Biology 2019, 74-75: 25-31

ISSUE DATE:

2019-07

URL:

<http://hdl.handle.net/2433/243897>

RIGHT:

© 2019. This manuscript version is made available under the CC-BY-NC-ND 4.0 license  
<http://creativecommons.org/licenses/by-nc-nd/4.0/>; The full-text file will be made open to the public on 1 July 2020 in accordance with publisher's 'Terms and Conditions for Self-Archiving'; This is not the published version. Please cite only the published version.; この論文は出版社版ではありません。引用の際には出版社版をご確認ください。

1    **Evaluation of [ $^{18}\text{F}$ ]pitavastatin as a positron emission tomography probe for *in vivo***  
2    **organic transporter polypeptide function**

3  
4    Yusuke Yagi<sup>a,b#</sup>, Hiroyuki Kimura<sup>a,b#\*</sup>, Haruka Okuda<sup>a</sup>, Masahiro Ono<sup>a</sup>, Yuji Nakamoto<sup>c</sup>,  
5    Kaori Togashi<sup>c</sup>, Hideo Saji<sup>a\*</sup>

6  
7    <sup>a</sup>Department of Patho-Functional Bioanalysis, Graduate School of Pharmaceutical Sciences,  
8    Kyoto University, 46-29 Yoshida Shimoadachi-cho, Sakyo-ku, Kyoto 606-8501, Japan

9    <sup>b</sup>Department of Analytical and Bioinorganic Chemistry, Kyoto Pharmaceutical University, 5  
10    Nakauchi-cho, Misasagi, Yamashina-ku, Kyoto 607-8414, Japan

11    <sup>c</sup>Department of Diagnostic Imaging and Nuclear Medicine, Kyoto University Graduate  
12    School of Medicine, 54 Shogoin Kawahara-cho, Sakyo-ku, Kyoto 606-8507, Japan

13  
14    <sup>#</sup>These authors contributed equally to this work.

15  
16    \*Corresponding authors:

17    Hiroyuki Kimura, PhD and Hideo Saji, PhD

18    Department of Patho-Functional Bioanalysis, Graduate School of Pharmaceutical Sciences,  
19    Kyoto University; 46-29 Yoshida Shimoadachi-cho, Sakyo-ku, Kyoto 606-8501, Japan

- 1 Tel: +81-75-753-4556, Fax: +81-75-753-4568
- 2 E-mail: [hkimura@mb.kyoto-phu.ac.jp](mailto:hkimura@mb.kyoto-phu.ac.jp), [hsaji@pharm.kyoto-u.ac.jp](mailto:hsaji@pharm.kyoto-u.ac.jp)
- 3

## 1    **Abstract**

2    **Introduction:** To understand the pathways involved in drug clearance from the body,  
3    quantitative evaluations of the hepatobiliary transport of drugs are important. The organic  
4    anion transporting polypeptide (OATP) family transporter, particularly OATP1B1 and 1B3,  
5    are considered to play an important role in hepatic uptake of organic anion compounds.  
6    Pitavastatin is a substrate of OATP, and it includes a fluorine group. Therefore, it represents  
7    an acceptable positron-emission tomography (PET) probe using F-18 to image in vivo hepatic  
8    transporter functions.

9    **Method:** [ $^{18}\text{F}$ ]Pitavastatin was synthesized using the method we previously reported. To  
10    evaluate the potential of [ $^{18}\text{F}$ ]pitavastatin in PET imaging of in vivo OATP functions, we  
11    investigated the hepatic uptake with/without rifampicin as an OATP inhibitor after  
12    administration in normal SD rats. [ $^{18}\text{F}$ ]Pitavastatin metabolite was evaluated using  
13    reverse-phase thin-layer chromatography (TLC) autoradiography. We subsequently analyzed  
14    the PET image results and demonstrated that [ $^{18}\text{F}$ ]pitavastatin selectively accumulated in the  
15    liver post-administration.

16    **Result and discussion:** In metabolite analysis using reverse-phase TLC, we found that the  
17    radioactivity detected in the plasma, liver (>90% intact), and bile mostly originated from the  
18    parent pitavastatin of the PET study (~40 min). [ $^{18}\text{F}$ ]pitavastatin's hepatic uptake decreased  
19    (approximately 76%) with rifampicin co-administration in PET analysis. Because



[<sup>18</sup>F]pitavastatin has lower clearance in rats than other previously reported OATP1B PET probes, it holds the potential of an imaging probe that has a higher sensitivity in monitoring hepatic OATP1B function's changes.

**Conclusion:** Compared with the previously reported OATP imaging probes, [<sup>18</sup>F]pitavastatin is more suitable for the sensitive detection of functional changes in OATP transporters. We believe that [<sup>18</sup>F]pitavastatin enables quantitative analysis of the hepatobiliary transport system for organic anion compounds.

## Keywords

Organic anion transporting polypeptide; Positron-emission tomography; Fluorine-18; Pitavastatin; Integration plot method

## Abbreviations

*MRP2* multidrug resistance-associated protein 2, *OATP* organic anion transporting polypeptide, *%ID* percentage of injected dose, *PET* positron-emission tomography, *ROI* region of interest

## 1 Introduction

2 The assessment of hepatobiliary drug transport represents an important factor in  
3 understanding the pathways involved in drug clearance from the body. In humans, numerous  
4 uptake and efflux transporters are coordinately involved in the hepatobiliary transport of  
5 drugs [1,2]. The organic anion transporting polypeptide (OATP) family transports substrates  
6 in a Na<sup>+</sup> ion-independent manner [3]. In particular, the OATPs 1B1 and 1B3 play an  
7 important role in the hepatic uptake of organic anion compounds. These transporters are  
8 selectively expressed in the human liver. Of note, they recognize substrates that have anions  
9 of extremely diverse structures. Among the substrates, several drugs used in the clinic can be  
10 identified (e.g., 3-hydroxy-3-methylglutaryl-coenzyme A (HMG-CoA) reductase inhibitors  
11 (statins), angiotensin-converting enzyme inhibitors, angiotensin II receptor antagonists  
12 (sartans), and various anticancer drugs) [4]. Altered functions of these transporters, caused by  
13 drug–drug interactions and genetic polymorphisms of specific transporter isoforms, result in  
14 changes not only of blood–drug concentrations but also of intrahepatic drug concentrations.  
15 Based on the extended clearance concept, At present, human liver samples (i.e., frozen  
16 hepatocytes and liver tissue blocks) are available, and prediction of liver uptake in humans is  
17 possible. However, there is the need for the development of a more accurate quantification  
18 method.

1 Nuclear medicine imaging technology is attracting attention as a functional diagnostic  
2 method that enables noninvasive and specific molecular imaging with high sensitivity in  
3 living systems. Among others, positron-emission tomography (PET) is superior to  
4 single-photon emission computed tomography in terms of sensitivity and quantitative  
5 analysis. In recent years, several PET probes (e.g., [ $^{11}\text{C}$ ]15R-TIC [5, 6],  
6 [ $^{11}\text{C}$ ]dehydropravastatin [7, 8], [ $^{11}\text{C}$ ]telmisartan [9], [ $^{11}\text{C}$ ]rosuvastatin [10], and [ $^{18}\text{F}$ ]LCATD  
7 [11]) have been developed to directly characterize in vivo the hepatobiliary transport systems  
8 for organic anions (Figure 1) [6]. An important feature of PET probes for the quantification  
9 of transport functions is that the probes themselves must not undergo extensive metabolism.  
10 Otherwise, the pharmacokinetic parameters determined represent a complex of intrinsic  
11 parameters for metabolism and membrane transport.

12 In addition, almost developed PET probes used to examine hepatobiliary transport were  
13 previously labeled with  $^{11}\text{C}$ . While handling these compounds, time constraints were  
14 considered. The higher achievable activity for production and the longer half-lives of  
15  $^{18}\text{F}$ -labeled probes are clear advantages over  $^{11}\text{C}$ -probes for both pre-clinical and clinical PET  
16 imaging. As a consequence, there still exists a need to develop  $^{18}\text{F}$ -labeled compounds with  
17 longer half-lives. However, till date,  $^{18}\text{F}$ -tracer has only been developed as  $^{18}\text{F}$ -labeled bile  
18 acid derivative [ $^{18}\text{F}$ ]LCATD. In the present study, pitavastatin, an antihyperlipidemic agent,  
19 was selected as the maternal compound for the PET imaging probe. Pitavastatin clears

1 predominantly from the liver, where OATP1B1 and OATP1B3 play pivotal roles in its uptake  
2 [12]. As a consequence, pitavastatin is expected to have a unique pharmacokinetic character.  
3 Pitavastatin has a fluorine group in its structure. Therefore, by using  $^{18}\text{F}$ , a PET nuclide, a  
4 PET imaging probe can be made while maintaining the physical and chemical properties. In  
5 an earlier study, we developed a synthetic method of [ $^{18}\text{F}$ ]pitavastatin using the Suzuki  
6 coupling reaction with 4- $^{18}\text{F}$ fluoroiodobenzene ([ $^{18}\text{F}$ ]FIB) [13] (Figure 1). In the present  
7 study, we aimed at characterizing the hepatobiliary transport of [ $^{18}\text{F}$ ]pitavastatin in rats by  
8 PET imaging with co-administration of rifampicin, a typical OATP1B inhibitor.

9  
10

## 1    **Materials and Methods**

### 2    ***Materials***

3    All reagents and solvents used in the present study were commercially available. Specifically,  
4    we purchased them from Wako Pure Chemical Industries (Tokyo, Japan), Nacalai Tesque  
5    (Kyoto, Japan), Merck (Darmstadt, Germany), and Sigma Aldrich (St. Louis, MO, USA).  
6    Reagents and solvents were used as received, without further purification. The identity and  
7    concentration of [ $^{18}\text{F}$ ]pitavastatin were assessed by high-performance liquid chromatography.  
8    To this end, we used a Shimadzu system (a LC-20AT pump with an SPD-20A UV detector,  
9     $\sigma=220, 254\text{nm}$ ; Shimadzu, Kyoto, Japan) with a Cosmosil 5C18-AR-II column ( $4.6 \times 150$   
10    mm and  $10 \times 250$  mm; Nacalai Tesque) and a radioisotope detector.

11

### 12    ***Synthesis of [ $^{18}\text{F}$ ]pitavastatin***

13    [ $^{18}\text{F}$ ]Pitavastatin was synthesized as previously reported [13].

### 14    **Radiochemistry**

15    [ $^{18}\text{F}$ ]Fluoride was produced using a cyclotron (CYPRIS HM-18, Sumitomo Heavy Industries,  
16    Tokyo, Japan) via an  $^{18}\text{O}$  (p,n)  $^{18}\text{F}$  reaction and passed through a Sep-Pak Light QMA  
17    cartridge (Waters Corporation, Milford, MA, USA) as an aqueous solution in  $^{18}\text{O}$ -enriched  
18    water. The cartridge was then dried using  $\text{N}_2$ , and  $^{18}\text{F}$  activity was eluted using 1.0 mL of a  
19    Kryptofix2.2.2 (Merck)/ $\text{K}_2\text{CO}_3$  solution [9.5 mg of Kryptofix2.2.2 and 1.7 mg of  $\text{K}_2\text{CO}_3$  in  
20    MeCN/water (96/4)]. The solvent was removed by azeotropic dehydration with MeCN (1.0  
21    mL) at  $120^\circ\text{C}$  under a stream of argon gas for 10 min.

### 22    **Synthesis of 4- $^{18}\text{F}$ Fluoroiodobenzene**

1 A solution of 4-iodophenyldiphenylsulfonium triflate (2.00 mg) in MeCN (150  $\mu$ L) was  
2 added to a reaction vessel containing the  $^{18}\text{F}$  activity (1.10–1.50 GBq), and the reaction  
3 mixture was heated for 1 min under microwave irradiation (50.0 W). The resulting mixture  
4 was cooled for 1 min and then passed through a Sep-Pak Light C18 column (Waters) and  
5 washed with water (10 mL). A stream of  $\text{N}_2$  gas was passed over the column for 10 s, and  
6 4- $^{18}\text{F}$ fluoroiodobenzene was eluted using MeCN (500  $\mu$ L). The eluent containing  
7 4- $^{18}\text{F}$ fluoroiodobenzene was purified using HPLC [radiochemical yield  $56.2\% \pm 3.1\%$   
8 decay corrected, data are the mean  $\pm$  SD ( $n = 3$ )].

#### 9 **Synthesis of $^{18}\text{F}$ pitavastatin using the Suzuki-coupling**

10 A solution of  $^{18}\text{F}$ fluoroiodobenzene in MeCN (185–222 MBq, 100–150  $\mu$ L) was added to a  
11 solution of boronic ester precursor (2.0 mg), tris(dibenzylideneacetone)dipalladium(0) (1.0  
12 mg) and cesiumcarbonate (4.0 mg) in MeCN (100  $\mu$ L); the resulting mixture was heated to  
13  $100^\circ\text{C}$  under microwave irradiation (50.0 W) for 1 min. The mixture was then passed through  
14 the COSMONICE(R) Filter (S) (0.45  $\mu\text{m}$ , 4 mm) and purified using preparative HPLC  
15 [Cosmosil 5C18-ARII 10  $\times$  250 mm column, MeOH/20 mM phosphate buffer (pH 2.5) =  
16 70/30, flow rate 5.0 mL/min] to obtain a pure solution of  $^{18}\text{F}$ pitavastatin [ $R_t = 8.5$  min,  
17 radiochemical yield:  $12.1\% \pm 3.0\%$  decay corrected from  $^{18}\text{F}$ fluoride ions (mean  $\pm$  SD,  $n =$   
18 3), radiochemical purity:  $>99\%$ , molar activity:  $>10.0$  GBq/ $\mu\text{mol}$ ].

19

## 1    *Animals*

2    Male Sprague Dawley (SD) rats weighing 222–333 g (8–10 weeks old) were purchased from  
3    Japan SLC, Inc. (Shizuoka, Japan). All animals were kept in a temperature- and  
4    light-controlled environment with standard food. Tap water was provided ad libitum. All  
5    animal procedures were approved by the Kyoto University Animal Care Committee.

## 7    *PET Scans*

8    All PET and computed tomography (CT) scans were performed using a FX-3300 (Gamma  
9    Medica, Salem, NH, USA), specifically designed for laboratory animals. Specifically, this  
10    PET scanner has a spatial resolution of <1 mm in full width at half-maximal at the center of  
11    the view at 100 mm in diameter and an axial extent of 110 mm in length. Control SD rats  
12    were used for PET experiments with [<sup>18</sup>F]pitavastatin alone. Rats were anesthetized and  
13    maintained under anesthesia with 1.5% isoflurane. Additionally, the femoral artery was  
14    cannulated with polyethylene tubing for blood collection. At the start of the emission scan,  
15    [<sup>18</sup>F]pitavastatin was administered as a single bolus (<85.1 nmol) via the tail vein [dosage:  
16    7.06 ± 1.49 MBq; data are presented as mean ± SD (n = 3)]. All PET acquisitions were  
17    performed in dynamic scan mode for 60 min. Conversely, we intravenously infused  
18    rifampicin, a typical inhibitor of OATP1Bs, to estimate the transport function of OATP1Bs in  
19    the liver as an OATP inhibition model [7]. Rifampicin infusion occurred at a rate of 1.5

1     $\mu\text{mol}/\text{min}/\text{kg}$  for at least 90 min prior to the administration of [ $^{18}\text{F}$ ]pitavastatin. Additionally,  
2    a constant infusion rate was maintained until the PET scan was concluded (in total, 50–75  
3     $\mu\text{mol}$  of rifampicin was used for blocking scan). Blood sampling time points were as follows:  
4    10, 20, 30, 40, and 50 s and 1, 2, 5, 10, 20, and 30 min after bolus administration of  
5    [ $^{18}\text{F}$ ]pitavastatin. Additionally, the total blood volume sampled from each rat was maximum  
6    160  $\mu\text{L}$ , which did not exceed 1% of the total circulating blood volume (1.6 mL) as  
7    approximately 10  $\mu\text{L}$  of blood was sampled at each time point. Of note, such blood sampling  
8    causes very less damage in rats. Blood radioactivity levels were measured using a  $\mu\text{FmPC}$   
9    system (Shimadzu). Radioactivity in each measured sample was corrected for decay.  
10    Following the PET scan, CT scans were performed. To this end, the following conditions  
11    were used: tube voltage, 60 kV; tube current, 310  $\mu\text{A}$ . Anesthesia was maintained at 1.5%  
12    isoflurane pre-euthanasia, using an injection of sodium pentobarbital.

#### 14    *Analysis of PET Imaging*

15    PET images were reconstructed by Fourier rebinning and standard 3D ordered-subset  
16    expectation maximization. Regions of interest (ROIs) representing the liver were delineated  
17    using the Pmod program (v. 3.3; PMOD Technologies, Zurich, Switzerland). All the ROIs  
18    were combined and transformed to volumetric ones. The time-radioactivity curve for the liver



1 was performed by normalizing decay-corrected time-radioactivity measurements to  
2 [ $^{18}\text{F}$ ]pitavastatin's injected dose (% dose).

3

#### 4 ***Biodistribution of Radioactivity After [ $^{18}\text{F}$ ]pitavastatin Administration***

5 Rats were injected in the tail vein with a saline solution of [ $^{18}\text{F}$ ]pitavastatin. Animals were  
6 sacrificed at specific time points [i.e., 2, 5, 10, 15, 30, and 60 min postinjection; data are  
7 presented as mean  $\pm$  SD (n = 5)]. We quickly removed samples of the blood, heart, lung, liver,  
8 spleen, pancreas, stomach, intestine, kidney, bone, and whole brain. The tissues' radioactivity  
9 was measured with a 1480 WIZARD 3 automatic gamma counter (PerkinElmer Co., Ltd.).  
10 Finally, results were expressed as the percentage of the injected dose (%ID). All radioactivity  
11 measurements were corrected for decay.

12

#### 13 ***Analysis of Metabolites in the Blood, Bile, and Liver Using Thin-Layer Chromatography*** 14 ***(TLC)***

15 Metabolite analysis was executed as previously described [6]. We first performed cannulation  
16 of the femoral artery and the bile duct in the SD rat. Then, [ $^{18}\text{F}$ ]pitavastatin was injected via  
17 the tail vein at a dosage of 40MBq. Arterial blood samples were collected at 1, 2, 5, 10, 20,  
18 and 40 min postinjection. Additionally, bile samples were collected at 0–5, 5–10, 10–25, and  
19 25–40 min postinjection. In order to perform liver tissue sampling, blood flow was

terminated by transection of the abdominal aorta and vein at 10 and 40 min postinjection. The liver was then quickly removed and homogenized. Additionally, precipitation with acetonitrile was used to deproteinize blood, bile, and liver samples. After centrifugation (12000 rpm, 2 min, 0°C), the supernatants were applied to RP-18 TLC plates (Merck KGaA, Darmstadt, Germany). Plates were developed at room temperature using acetonitrile/water/acetic acid (50:50:0.75) as a mobile phase. After migration, plates were dried and exposed to BAS SR2040 imaging plates (Fuji Film, Tokyo, Japan) for 90–360 min. Radioactivity's distribution on the imaging plates was determined by digital PSL autoradiography using a Fuji BAS-5000 analyzer. Subsequently, data was analyzed using the MultiGauge image analysis program (Fuji Film). Rf value was determined pitavastatin and a lactone form of pitavastatin which was synthesized [13].

#### ***Kinetic Analyses of PET Data to Determine the Clearance of Radioactivity***

Radioactivity's initial uptake clearance in the liver ( $CL_{\text{uptake,liver}}$ ) was calculated by integration plot analyzes [14]. To this end, the initial linear portion of the curves after [ $^{18}\text{F}$ ]pitavastatin administration (0.5–5 min) was used. The  $CL_{\text{uptake,liver}}$  of [ $^{18}\text{F}$ ]pitavastatin was estimated based on the following equation:

$$\frac{X_{t,\text{liver}}}{C_{t,\text{blood}}} = CL_{\text{uptake,liver}} \times \frac{AUC_{0-t,\text{blood}}}{C_{t,\text{blood}}} + V_{E,\text{liver}}, \quad (1)$$

1 where  $X_{t,liver}$ ,  $C_{t,blood}$ , and  $AUC_{0-t,blood}$  represent the amount of radioactivity in the liver at time  
2  $t$ , the blood concentration of radioactivity at time  $t$ , and the area under the blood  
3 concentration–time curve from time 0 to  $t$ , respectively.  $V_{E,liver}$  represents the initial  
4 distribution volume in the liver at time 0. This was calculated from the y intercept of the  
5 integration plot. To estimate  $AUC_{0-t,blood}$ , radioactivity’s blood concentration–time curve was  
6 fitted to the following two-exponential equation:

$$7 \quad C_{B,t} = Ae^{-\alpha t} + Be^{-\beta t}$$

8 to optimize parameters ( $\alpha$ ,  $\beta$ , A, B). Then,  $AUC_{0-t,blood}$  was calculated by means of the  
9 following equation:

$$10 \quad AUC_{0-t,blood} = \frac{A}{\alpha} \cdot (1 - e^{-\alpha t}) + \frac{B}{\beta} \cdot (1 - e^{-\beta t}) \quad (2)$$

11  $CL_{uptake,liver}$  was obtained from the initial slope of the plot of  $X_{t,liver}/C_{t,blood}$  versus  
12  $AUC_{0-t,blood}/C_{t,blood}$ .

13

## 14 ***Statistical Analysis***

15 Student’s two-tailed  $t$ -test was used to identify significant differences in the kinetic  
16 parameters between control and rifampicin-treated rats. We considered as statistically  
17 significant  $p$ -values  $<0.05$ .

18

19

## 1 Results and Discussion

### 2 *Radiometabolite Analysis of [<sup>18</sup>F]pitavastatin in the Blood, Liver, and Bile by TLC*

#### 3 *Autoradiography*

4 Figure 2 shows TLC radiograms in which the extract from plasma, liver, and bile after  
5 [<sup>18</sup>F]pitavastatin administration was developed by reverse-phase TLC, respectively. In the  
6 present study, we showed that virtually no metabolites were detectable in the blood. When  
7 evaluating the liver extracts, we found that one metabolite (M1) was barely detectable  
8 following the administration of [<sup>18</sup>F]pitavastatin. However, almost all radioactivity was  
9 derived from intact [<sup>18</sup>F]pitavastatin (94.6% at 40 min, Supplemental table 1). As for bile  
10 extracts, we identified a lactone form of pitavastatin [13] and two metabolites (M1 and M2).  
11 However, 81.9% of the radioactivity was derived from intact [<sup>18</sup>F]pitavastatin, 40 min after  
12 [<sup>18</sup>F]pitavastatin administration (Supplemental table 1).

13 Results of this study showed that [<sup>18</sup>F]pitavastatin's metabolite analysis was in line with  
14 previous reports on [<sup>14</sup>C]pitavastatin [15, 16]. In the case of [<sup>14</sup>C]pitavastatin, a previous  
15 study showed that 84, 95, and 85% of the total radioactivity was derived from pitavastatin in  
16 the plasma, liver, and bile 60 min post-intravenous administration of [<sup>14</sup>C]pitavastatin,  
17 respectively [15, 16]. Of note, these results indicated that most of the radioactivity was  
18 derived from [<sup>18</sup>F]pitavastatin. Therefore, we believe that the kinetic parameters estimated  
19 from the present PET study correctly reflect pitavastatin's hepatobiliary transport.

# ***Biodistribution of Radioactivity and Effect of Rifampicin Co-administration in the Abdominal Region Post-intravenous Administration of [<sup>18</sup>F]pitavastatin***

Figure 3 shows the PET image of normal SD rat with/without rifampicin as an OATP inhibitor after [<sup>18</sup>F]pitavastatin administration. Additionally, it presents the analysis results from PET images using the Pmod program. In the control rats' liver, a maximum of 48.1±1.5% of the injected dose was distributed 8 min post-administration of [<sup>18</sup>F]pitavastatin. Additionally, we found a decrease of radioactivity until the PET scan's end (39.3±1.27%ID at 30 min). Results of the biodistribution study in normal SD rats over time showed that radioactivity was predominantly present in the liver in the early phase (71.5±3.4%ID at 10 min, Table 1). It then gradually decreased by the end of the examination (54.1±5.1%ID at 30 min). Additionally, we observed that radioactivity's reduction rates in the liver were similar among PET scan and biodistribution study. Furthermore, data error was small. These results suggest that the PET analysis of [<sup>18</sup>F]pitavastatin was appropriately consistent compared with the biodistribution study. On the contrary, radioactivity was also detected post-administration of [<sup>18</sup>F]pitavastatin in the kidney at early time points and in the intestine at a later time point (30 min). However, similarly to a separate conventional biodistribution study, in the PET scan, no clear distribution of radioactivity to other tested organs was observed (Table 1). These results are consistent with a previous study of [<sup>14</sup>C]pitavastatin. Specifically, an earlier whole-body autoradiography of rats that received an intravenous administration of

1  $[^{14}\text{C}]$ pitavastatin indicated that radioactivity mainly accumulated in the liver and kidney at  
2 2.5 min, while high levels of radioactivity were found in the liver and intestine 60 min  
3 post-administration [15, 16]. We think that OATP1A2 expressed in the kidney affected early  
4 uptake of pitavastatin as this drug has less contribution to OATP1A2 compared with that to  
5 OATP1B1 [3, 17, ]. In rifampicin-treated rats, as shown in Figure 3, we found that the  
6 amount of radioactivity accumulated in the liver and intestine was noticeably less than in  
7 control rats (no rifampicin). Furthermore, the liver's maximum radioactivity ( $31.6 \pm 4.9\%$  at  
8 8 min) decreased to 65% compared with control rats ( $p < 0.05$ ; Student's two-tailed  $t$ -test).  
9 Such results suggested that the hepatobiliary transport of  $[^{18}\text{F}]$ pitavastatin was modified by  
10 co-administration with rifampicin, an OATP inhibitor. On the contrary, radioactivity's blood  
11 concentration became significantly higher even 2 min after  $[^{18}\text{F}]$ pitavastatin administration vs.  
12 control rats. Furthermore, radioactivity levels in the liver and intestine were found to be  
13 significantly lower. In the present study, the protocol of rifampicin administration used  
14 (constant infusion of  $1.5 \mu\text{mol}/\text{min}/\text{kg}$  for  $>90$  min) was the same as the one used in previous  
15 PET studies with  $[^{11}\text{C}]$ dehydropravastatin and  $[^{11}\text{C}]$ telmisartan [7, 9]. Specifically, unbound  
16 blood concentration of rifampicin was 11–13  $\mu\text{M}$  at steady state in rats. This value is  
17 sufficiently high to potently inhibit rat Oatp1a4 ( $K_i = 1.46 \mu\text{M}$ ) and Oatp1b2 ( $K_i = 0.79 \mu\text{M}$ )  
18 and to partly inhibit rat Oatp1a1 ( $K_i = 18.2 \mu\text{M}$ ) [18, 19].

19

# 1 *Kinetic Analyses of PET Data to Determine Radioactivity's Clearance*

2 Radioactivity in blood samples was eliminated in a biphasic manner in both control and  
3 rifampicin-treated rats (Fig. 3C). However, with co-administration of rifampicin,  
4 radioactivity's elimination was delayed. Additionally, its blood  $AUC_{0-30}$ , normalized by  
5  $[^{18}F]$ pitavastatin's dose, was 3.4-fold larger in rifampicin-treated rats [ $111.4 \pm 34.9$  (% of  
6 dose/mL\*min)] than in control SD rats [ $33.1 \pm 5.0$  (% of dose/mL\*min);  $p < 0.05$ ; Student's  
7 two-tailed  $t$ -test]. Similarly, these results indicate that blood concentration increased due to  
8 liver uptake inhibition by rifampicin. Integration plots for hepatic uptake clearance  
9 ( $CL_{\text{uptake,liver}}$ ) are shown in Figure 4A, and their kinetic parameters are summarized in Figure  
10 4B. Linearity of the plot was maintained for a short time period between 0.5–5 min for liver  
11 uptake. In control rats,  $CL_{\text{uptake,liver}}$  was  $9.08 \pm 1.33$  mL/min/kg, while in rifampicin-treated  
12 rats,  $CL_{\text{uptake,liver}}$  significantly decreased to 26% of the control values ( $2.33 \pm 0.11$  mL/min/kg,  
13  $p < 0.05$ ; Student's two-tailed  $t$ -test). Of note, the degree of decrease in  $CL_{\text{uptake,liver}}$  of  
14  $[^{18}F]$ pitavastatin was noticeably smaller with respect to previous reported probes as  
15  $[^{11}C]$ telmisartan (65% of control) and  $[^{11}C]$ dehydropravastatin (69% of control) [7, 9]. These  
16 differences can partially be explained by the fact that the  $CL_{\text{uptake,liver}}$  values of  
17  $[^{11}C]$ telmisartan ( $63 \pm 11$  mL/min/kg) [7] and  $[^{11}C]$ dehydropravastatin ( $73.6 \pm 4.8$   
18 mL/min/kg) [9] were almost equal to the hepatic blood flow rate (55 mL/min/kg). This result  
19 implies that it was difficult to accurately calculate the intrinsic hepatic uptake clearance in

1 rats [20, 21]. Conversely, this value of [ $^{18}\text{F}$ ]pitavastatin ( $9.08 \pm 1.33$  mL/min/kg) was  
2 one-sixth of the hepatic blood flow rate. Therefore, we believe that [ $^{18}\text{F}$ ]pitavastatin can be  
3 used to estimate the intrinsic hepatic uptake clearance in rats in an *in vivo* PET study.  
4 Furthermore, pitavastatin's *in vitro* uptake clearance in rat hepatocytes was reported to be  
5 121–444  $\mu\text{L}/\text{min}/\text{mg}$  protein [22, 23]. The latter corresponds to a  $\text{CL}_{\text{uptake, liver}}$  of 10.4–26.1  
6 mL/min/kg, assuming a well-stirred model with physiological scaling factors ( $1.2 \times$   
7  $10^8$  cells/g liver, 41.2 g liver/kg;  $f_B$  of pitavastatin in rats, 0.021) [23, 24]. Thus, hepatic  
8 clearance determined from the *in vitro* study of pitavastatin is similar to that determined from  
9 the PET analysis of [ $^{18}\text{F}$ ]pitavastatin. As a result, [ $^{18}\text{F}$ ]pitavastatin has the potential of a  
10 higher sensitivity in detecting the inhibitory effects of drugs on hepatic OATP1B transporters  
11 vs. other reported OATP imaging probes.

12

13



## 1    **Conclusion**

2    In summary, in the present feasibility study, the kinetic analyzes of [ $^{18}\text{F}$ ]pitavastatin's  
3    hepatobiliary transport in rats were carried out using PET imaging. As expected,  
4    intravenously infusion of rifampicin, a typical OATP inhibitor, reduced hepatic uptake. Such  
5    findings confirmed that, in the rat's liver, [ $^{18}\text{F}$ ]pitavastatin's membrane transport was  
6    predominantly transporter mediated. [ $^{18}\text{F}$ ]pitavastatin can quantitatively detect changes in the  
7    hepatobiliary transport of an OATP inhibition model of rats. Compared with previously  
8    reported OATP imaging probes, especially [ $^{11}\text{C}$ ]dehydropravastatin and [ $^{11}\text{C}$ ]telmisartan, we  
9    can found that [ $^{18}\text{F}$ ]pitavastatin is suitable for the sensitive detection of functional changes in  
10    OATP transporters. We believe that this finding is due to drug–drug interactions and genetic  
11    polymorphisms of specific transporter isoforms by [ $^{18}\text{F}$ ]pitavastatin. Of note,  
12    [ $^{18}\text{F}$ ]pitavastatin's hepatic clearance was not limited by hepatic blood flow rate. Pitavastatin  
13    has been used as an antihyperlipidemic drug for many years. We believe that the  
14    pharmacokinetic properties identified here are also applicable to humans. Specifically, we  
15    expect that [ $^{18}\text{F}$ ]pitavastatin performs similarly in detecting functional changes in OATP1Bs  
16    in human PET studies.

17

18

## 1    **Acknowledgements**

2    This work was supported in part by the Advanced Research for Medical Products Mining  
3    Program of the National Institute of Biomedical Innovation (NIBIO) [grant number 156147],  
4    a Grant-in-Aid for Young Scientists (A) [grant number JP25713046] and a Grant-in- Aid for  
5    Scientific Research (C) [grant number JP17K10377] from the Japan Society for the  
6    Promotion of Science, the Takeda Science Foundation, and a Research Grant for  
7    Nanotechnical Medicine from the Ministry of Health, Labour and Welfare of Japan  
8    [20100000000573].

9

## 10   **Funding**

11   The funders had no role in study design, data collection and analysis, decision to publish, or  
12   preparation of the manuscript.

13

## 1    **References**

- 2    [1] K. Yoshida, K. Maeda, Y. Sugiyama, Hepatic and intestinal drug transporters: prediction  
3    of pharmacokinetic effects caused by drug-drug interactions and genetic polymorphisms.  
4    Annu.                    Rev.                    Pharmacol.                    Toxicol.                    2013;53:581–612.  
5    <https://doi.org/10.1146/annurev-pharmtox-011112-140309>.
- 6    [2] M.J. Zamek-Gliszczyński, M.E. Taub, P.P. Chothé, et al., Transporters in drug  
7    development: 2018 ITC recommendations for transporters of emerging clinical importance.  
8    Clin. Pharmacol. Ther. 2018;104:890–899. <https://doi.org/10.1002/cpt.1112>
- 9    [3] A. Obaidat, M. Roth, B. Hagenbuch, The expression and function of organic anion  
10    transporting polypeptides in normal tissues and in cancer, Annu. Rev. Pharmacol. Toxicol.  
11    2012;52:135–151. <https://doi.org/10.1146/annurev-pharmtox-010510-100556>.
- 12    [4] K. Maeda, H. Suzuki, Y. Sugiyama, Hepatic Transport in: Drug Bioavailability  
13    Wiley-VCH            Verlag            GmbH;            2009,            chapter            11,            p            277–332.  
14    <https://doi.org/10.1002/9783527623860.ch11>.
- 15    [5] T. Takashima, S. Kitamura, Y. Wada, et al., PET imaging-based evaluation of  
16    hepatobiliary transport in humans with (15R)-<sup>11</sup>C-TIC-Me. J. Nucl. Med. 2012;53:741–748.  
17    <https://doi.org/10.2967/jnumed.111.098681>.
- 18    [6] T. Takashima, H. Nagata, T. Nakae, et al., Positron emission tomography studies using  
19    (15R)-16-m-[<sup>11</sup>C]tolyl-17,18,19,20-tetranorisocarbacyclin methyl ester for the evaluation of

- 1 hepatobiliary transport. J. Pharmacol. Exp. Ther. 2010;335:314–323.
- 2 <https://doi.org/10.1124/jpet.110.170092>.
- 3 [7] T. Shingaki, T. Takashima, R. Ijuin, et al., Evaluation of Oatp and Mrp2 activities in
- 4 hepatobiliary excretion using newly developed positron emission tomography tracer
- 5 [ $^{11}\text{C}$ ]dehydropravastatin in rats. J. Pharmacol. Exp. Ther. 2013;347:193–202.
- 6 <https://doi.org/10.1124/jpet.113.206425>.
- 7 [8] K. Kaneko, M. Tanaka, A. Ishii, et al., A clinical quantitative evaluation of hepatobiliary
- 8 transport of [ $^{11}\text{C}$ ]dehydropravastatin in humans using positron emission tomography. Drug.
- 9 Metab. Dispos. 2018;46:719–728. <https://doi.org/10.1124/dmd.118.080408>.
- 10 [9] T. Takashima, Y. Hashizume, Y. Katayama, et al., The involvement of organic anion
- 11 transporting polypeptide in the hepatic uptake of telmisartan in rats: PET studies with
- 12 [ $^{11}\text{C}$ ]telmisartan. Mol. Pharm. 2011;8:1789–1798. <https://doi.org/10.1021/mp200160t>.
- 13 [10] J. He, Y. Yu, B. Prasad, et al., PET imaging of Oatp-mediated hepatobiliary transport of
- 14 [ $^{11}\text{C}$ ]rosuvastatin in the rat. Mol. Pharm. 11 2014;11:2745–2754.
- 15 <https://doi.org/10.1021/mp500027c>.
- 16 [11] A. Testa, S. Angelo, M. Mingarelli, et al., Design, synthesis, in vitro characterization and
- 17 preliminary imaging studies on fluorinated bile acid derivatives as PET tracers to study
- 18 hepatic transporters. Bioorg. Med. Chem. 2017;25:963–976.
- 19 <https://doi.org/10.1016/j.bmc.2016.12.008>.

- 1 [12] M. Hirano, K. Maeda, Y. Shitara, et al., Contribution of OATP2 (OATP1B1) and
- 2 OATP8 (OATP1B3) to the hepatic uptake of pitavastatin in humans. *J. Pharmacol. Exp. Ther.*
- 3 2004;311:139–146. <https://doi.org/10.1124/jpet.104.068056>.
- 4 [13] Y. Yagi, H. Kimura, K. Arimitsu, et al., The synthesis of [ $^{18}\text{F}$ ]pitavastatin as a tracer for
- 5 hOATP using the Suzuki coupling. *Org. Biomol. Chem.* 2015;13:1113–1121.
- 6 <https://doi.org/10.1039/c4ob01953a>.
- 7 [14] D. C. Kim, Y. Sugiyama, M. Hanano, Kinetic analysis of in vivo receptor-dependent
- 8 binding of human epidermal growth factor by rat tissues. *J. Pharm. Sci.* 1988;77 (3):200–207.
- 9 <https://doi.org/10.1002/jps.2600770304>
- 10 [15] H. Kimata, H. Fujino, T. Koide, et al., Studies on the metabolic fate of NK-104, a new
- 11 inhibitor of HMG-CoA reductase (1): absorption, distribution, metabolism and excretion in
- 12 Rats. *Drug. Metab. Pharmacokinet.* 1998;13:484–499. <https://doi.org/10.2133/dmpk.13.484>.
- 13 [16] H. Fujino, Y. Tsunenari, T. Koide, et al., Studies on the Metabolic Fate of NK-104, a
- 14 New Inhibitor of HMG-CoA Reductase. (2). Absorption, Distribution, Metabolism, Excretion
- 15 and Accumulation Following Repeated Oral Administration of  $^{14}\text{C}$ -NK-104 in Rats. *Drug.*
- 16 *Metab. Pharmacokin.* 1998;13(5):499–507. <https://doi.org/10.2133/dmpk.13.499>
- 17 [17] Y. Shirasaka, K. Suzuki, M. Shichiri, et al., Intestinal absorption of HMG-CoA
- 18 reductase inhibitor pitavastatin mediated by organic anion transporting polypeptide and

- 1 P-glycoprotein/multidrug resistance 1. *Drug Metab. Pharmacokinet.* 2011;26 (2):171–179.
- 2 <https://doi.org/10.2133/dmpk.DMPK-10-RG-073>
- 3 [18] Y. Shitara, D. Sugiyama, H. Kusuhashi, et al., Comparative inhibitory effects of different
- 4 compounds on rat oatpl (slc21a1)- and Oatp2 (Slc21a5)-mediated transport. *Pharm. Res.*
- 5 2002;19:147–153. <http://dx.doi.org/10.1023/A:1014264614637>.
- 6 [19] Y.Y. Lau, H. Okochi, Y. Huang, et al., Multiple transporters affect the disposition of
- 7 atorvastatin and its two active hydroxy metabolites: application of in vitro and ex situ systems.
- 8 *J. Pharmacol. Exp. Ther.* 2006;316:762–771. <https://doi.org/10.1124/jpet.105.093088>.
- 9 [20] M.S. Roberts, M. Rowland, Correlation between in - vitro microsomal enzyme activity
- 10 and whole organ hepatic elimination kinetics: analysis with a dispersion model. *J. Pharm.*
- 11 *Pharmacol.* 1986;38(3):177–181. <https://doi.org/10.1111/j.2042-7158.1986.tb04540.x>.
- 12 [21] T. Iwatsubo, N. Hirota, T. Ooie, et al., Prediction of in vivo drug metabolism in the
- 13 human liver from in vitro metabolism data. *Pharmacol. Ther.* 1997;73(2):147–171.
- 14 [https://doi.org/10.1016/S0163-7258\(96\)00184-2](https://doi.org/10.1016/S0163-7258(96)00184-2).
- 15 [22] S. Shimada, H. Fujino, T. Morikawa, et al., Uptake mechanism of pitavastatin, a new
- 16 inhibitor of HMG-CoA reductase, in rat hepatocytes. *Drug. Metab. Pharmacokinet.*
- 17 2003;18:245–251. <https://doi.org/10.2133/dmpk.18.245>.

- 1 [23] T. Watanabe, H. Kusuhara, K. Maeda, et al., Investigation of the rate-determining  
2 process in the hepatic elimination of HMG-CoA reductase inhibitors in rats and humans.  
3 Drug. Metab. Dispos. 2010;38:215–222. <https://doi.org/10.1124/dmd.109.030254>.
- 4 [24] T. Watanabe, H. Kusuhara, K. Maeda. et al., Physiologically based pharmacokinetic  
5 modeling to predict transporter-mediated clearance and distribution of pravastatin in humans.  
6 J. Pharmacol. Exp. Ther. 2009;328(2):652–662. <https://doi.org/10.1124/jpet.108.146647>  
7  
8  
9  
10

**Table 1.** Time-dependent tissue distribution of radioactivity after intravenous administration of [ $^{18}\text{F}$ ]pitavastatin.

	%ID/organ $\pm$ SD (n = 5)					
	2 min	5 min	10 min	15 min	30 min	60 min
Blood <sup>a</sup>	11.63 $\pm$ 1.31	4.57 $\pm$ 0.59	2.80 $\pm$ 0.21	1.97 $\pm$ 0.15	1.26 $\pm$ 0.16	1.35 $\pm$ 0.75
Heart	0.19 $\pm$ 0.01	0.12 $\pm$ 0.01	0.11 $\pm$ 0.01	0.11 $\pm$ 0.01	0.12 $\pm$ 0.02	0.12 $\pm$ 0.04
Lung	0.30 $\pm$ 0.02	0.18 $\pm$ 0.04	0.11 $\pm$ 0.02	0.09 $\pm$ 0.02	0.03 $\pm$ 0.01	0.06 $\pm$ 0.03
Liver	69.56 $\pm$ 1.66	70.11 $\pm$ 2.74	71.54 $\pm$ 3.40	68.05 $\pm$ 6.38	54.11 $\pm$ 5.13	32.61 $\pm$ 3.69
Pancreas	0.22 $\pm$ 0.08	0.06 $\pm$ 0.03	0.06 $\pm$ 0.02	0.05 $\pm$ 0.04	0.03 $\pm$ 0.02	0.04 $\pm$ 0.02
Spleen	0.08 $\pm$ 0.01	0.04 $\pm$ 0.01	0.02 $\pm$ 0.00	0.02 $\pm$ 0.01	0.01 $\pm$ 0.01	0.02 $\pm$ 0.02
Stomach	0.18 $\pm$ 0.03	0.29 $\pm$ 0.21	0.10 $\pm$ 0.10	0.34 $\pm$ 0.31	0.28 $\pm$ 0.33	0.12 $\pm$ 0.04
Intestine	4.00 $\pm$ 0.30	8.20 $\pm$ 0.90	13.33 $\pm$ 3.72	20.22 $\pm$ 2.79	33.78 $\pm$ 5.74	64.86 $\pm$ 7.72
Kidney	7.46 $\pm$ 0.37	2.13 $\pm$ 0.34	1.25 $\pm$ 0.27	0.97 $\pm$ 0.25	0.68 $\pm$ 0.10	0.55 $\pm$ 0.19
Bone <sup>b</sup>	0.12 $\pm$ 0.02	0.07 $\pm$ 0.01	0.04 $\pm$ 0.01	0.04 $\pm$ 0.02	0.04 $\pm$ 0.04	0.02 $\pm$ 0.03

<sup>a</sup> Assuming that weight of blood in rats was 10% of total body weight. <sup>b</sup> data is presented as %ID/g.



## 1 **Figure legends**

2 **Figure 1.** Chemical structure of the PET probe for OATP evaluation. (A) [ $^{11}\text{C}$ ]15*R*-TIC-Me,  
3 (B) [ $^{11}\text{C}$ ]dehydropravastatin, (C) [ $^{11}\text{C}$ ]telmisartan, (D) [ $^{11}\text{C}$ ]rosuvastatin, (E) [ $^{18}\text{F}$ ]pitavastatin  
4 (present study)

6 **Figure 2.** Representative TLC autoradiograms on the radio metabolite analysis following  
7 intravenous administration of [ $^{18}\text{F}$ ]pitavastatin in normal rat.  
8 Each line represents an authentic [ $^{18}\text{F}$ ]pitavastatin sample [pitavastatin (aus.)] and blood, liver,  
9 and bile extract samples collected at the designated time points following [ $^{18}\text{F}$ ]pitavastatin's  
10 intravenous administration. We have confirmed that pitavastatin lactone band's location is  
11 identical to the  $R_f$  values of the pitavastatin lactone that we created ( $R_f=0.13-0.14$ )

13 **Figure 3.** PET images of rat abdominal regions taken post-intravenous administration of  
14 [ $^{18}\text{F}$ ]pitavastatin (anesthesia: 1.5% isoflurane; dosage:  $7.06 \pm 1.49$  MBq;  $n = 3$ ). Colonal  
15 maximum intensity projecting PET images of radioactivity in the abdominal region were  
16 captured at 2, 5, 10, 20, and 30 min in control rats (A), rifampicin-treated rats at an infusion  
17 rate of  $1.5\mu\text{mol}/\text{min}/\text{kg}$  (B).

18 Radioactivity's time profiles in blood from the  $\mu\text{FmPC}$  system (C) and liver were determined  
19 by PET imaging analysis 30 min post-intravenous administration of [ $^{18}\text{F}$ ]pitavastatin. (D)  
20 Each symbol represents the control and rifampicin-treated rats ( $1.5\text{ mmol}/\text{min}/\text{kg}$  for at least a

1 90 min PET scan). The data represent the mean  $\pm$ SD. (n=3; Students *t*-test, \*  $p<0.05$ , † $<0.01$ ,  
2 ‡ $<0.005$ ) Inset figures show the data points within 5 min

3 **Figure 4.** (A) Integration plots were drawn for the calculation of hepatic uptake of total  
4 radioactivity in control and rifampicin-treated rats. The data represent the mean  $\pm$  SD (n=3).  
5 (B) [ $^{18}\text{F}$ ]pitavastatin's pharmacokinetic parameters after its intravenous administration in rats.  
6 The values represent the mean  $\pm$  SD (n=3; Students *t*-test, \*  $p<0.05$ )  
7

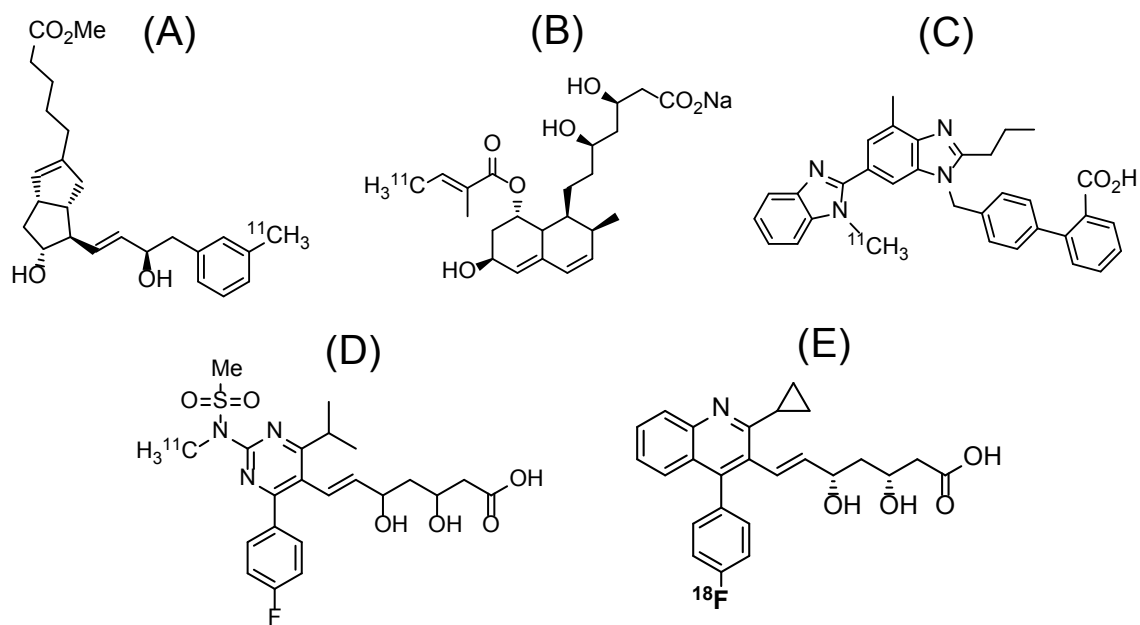


**Figure 1**

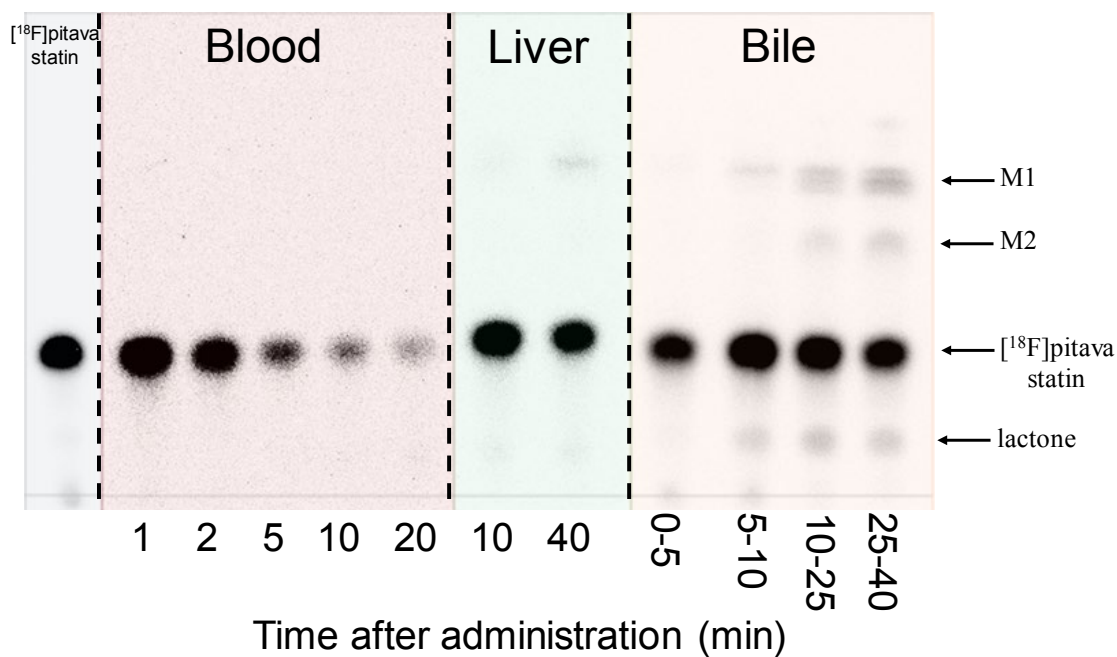


**Figure 2**

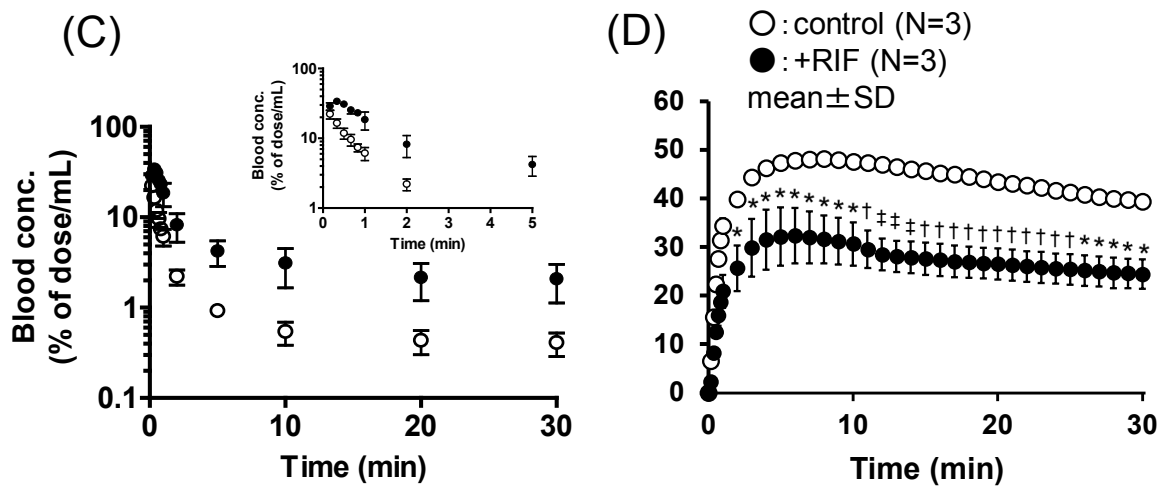
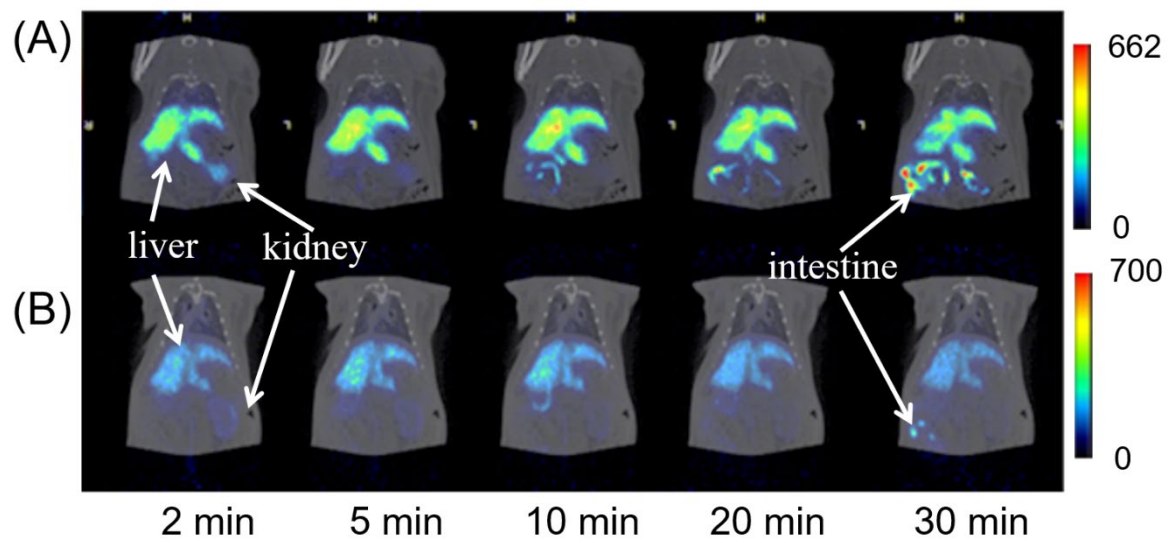


Figure 3

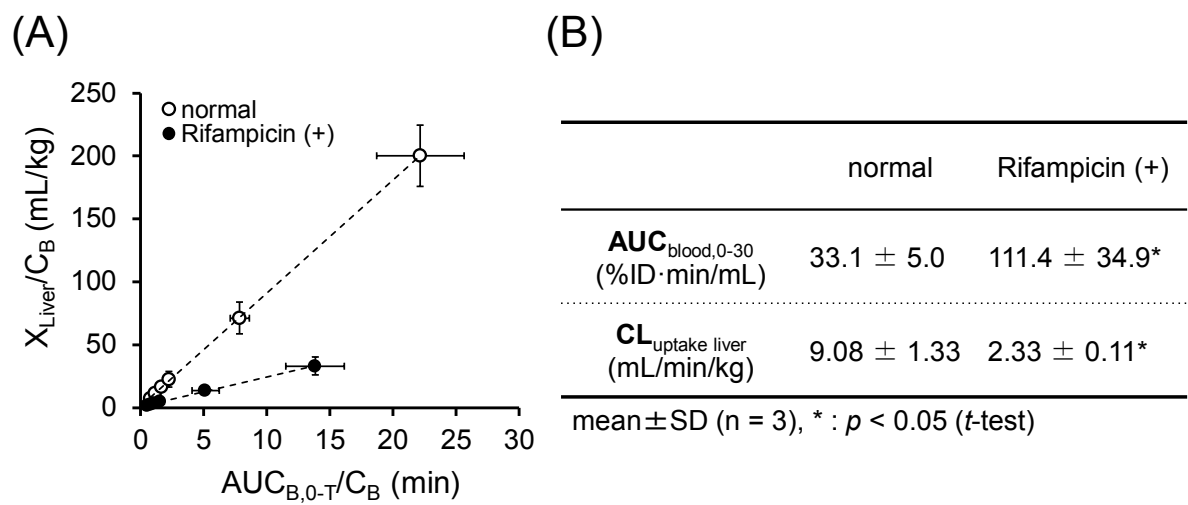


Figure 4